

Communication

# Study of Coarse Particle Types, Structure and Crystallographic Orientation Relationships with Matrix in Cu-Cr-Zr-Ni-Si Alloy

Chengdong Xia <sup>1</sup>, Chengyuan Ni <sup>1</sup>, Yong Pang <sup>1,\*</sup>, Yanlin Jia <sup>2</sup>, Shaohui Deng <sup>1</sup> and Wenhui Zheng <sup>1</sup><sup>1</sup> College of Mechanical Engineering, Quzhou University, Quzhou 324000, China; xcd309@163.com (C.X.)<sup>2</sup> School of Materials Science and Engineering, Central South University, Changsha 410083, China

\* Correspondence: thgink@126.com

**Abstract:** Coarse particles in Cu-0.39Cr-0.24Zr-0.12Ni-0.027Si alloy were studied with scanning electron microscopy and transmission electron microscopy. Three types of coarse particles were determined: a needle-like Cu<sub>5</sub>Zr intermetallic phase, a nearly spherical Cr<sub>9.1</sub>Si<sub>0.9</sub> intermetallic phase and (Cu, Cr, Zr, Ni, Si)-rich lath complex particles. The crystallographic orientation relationships of the needle-like and nearly spherical coarse particles were also determined. The reasons for formation and the role of the coarse phases in Cu-Cr-Zr alloys are discussed, and some suggestions are proposed to control the coarse phases in the alloys.

**Keywords:** Cu-Cr-Zr alloy; coarse particle; crystal structure; orientation relationship

## 1. Introduction

High-strength and high-electrical-conductivity copper alloys have been extensively used in railway contact wires [1,2], integrated circuit lead frame [3], heat exchangers [4] and other electrical and electronic engineering contexts [5]. These kinds of alloys have mainly included Cu-Fe systems, Cu-Ni systems, Cu-Cr systems and Cu-Mg systems [1–7], and Cu-Cr system alloys are potentially the most representative of copper alloys with the best balance of mechanical and electrical properties, especially Cu-Cr-Zr alloys [8–12]. In the past years, many investigations have focused on Cu-Cr-Zr alloys to improve physical and mechanical properties such as strength, conductivity, ductility and thermal stability with alloying, plastic deformation, rotary forging, friction stir processing and equal channel angular pressing [8–12], and the authors of this paper also carried out some studies in this field [13–16]. These previous studies have greatly promoted the developments and applications of Cu-Cr-Zr alloys in various fields.

It has been established unambiguously that Cu-Cr-Zr alloys are mainly strengthened by nanosized precipitates, and the characteristics of the nanosized precipitates such as structure, morphology, crystallographic orientation relationships and precipitation sequence were widely studied in the previous works [17–22]. It was reported that the microstructure had a bimodal particle distribution in Cu-Cr-Zr system alloys, while it has not been reported for the binary Cu-Cr alloy [23,24]. Therefore, some researchers studied the coarse particles in Cu-Cr-Zr system alloys [25–29]. Suzuki et al. [25] considered that the dispersed precipitates located on the {111} plane of Cu were Cu<sub>3</sub>Zr phase. Tang et al. [26] reported that intermetallic precipitates on the grain boundary in the Cu-Cr-Zr-Mg alloy were Cu<sub>4</sub>Zr. Huang et al. [27] concluded that the coarse intermetallic particles were Cu<sub>51</sub>Zr<sub>14</sub> with an hcp structure using transmission electron microscope (TEM) and energy dispersive spectroscopy (EDS) analysis. Theoretical studies conducted by Ge [28] and Cui [29] showed that the Cu<sub>51</sub>Zr<sub>14</sub>, Cu<sub>10</sub>Zr<sub>7</sub>, CuZr<sub>2</sub>, CuZr phase should exist in Cu-Zr metallic glass. Although the previous researchers confirmed that Cr particles and (Cu, Zr) particles were present in Cu-Cr-Zr system alloys by means of scanning electron microscope (SEM) and TEM investigations, there has been no accurate experimental evidence and unanimous agreement on



**Citation:** Xia, C.; Ni, C.; Pang, Y.; Jia, Y.; Deng, S.; Zheng, W. Study of Coarse Particle Types, Structure and Crystallographic Orientation Relationships with Matrix in Cu-Cr-Zr-Ni-Si Alloy. *Crystals* **2023**, *13*, 518. <https://doi.org/10.3390/cryst13030518>

Academic Editors: Andrea Di Schino and Claudio Testani

Received: 27 February 2023

Revised: 14 March 2023

Accepted: 15 March 2023

Published: 17 March 2023



**Copyright:** © 2023 by the authors. Licensee MDPI, Basel, Switzerland. This article is an open access article distributed under the terms and conditions of the Creative Commons Attribution (CC BY) license (<https://creativecommons.org/licenses/by/4.0/>).

the types and structure of coarse particles or their crystallographic orientation relationships with the matrix so far.

The present study focuses on the coarse particle types, structure and crystallographic orientation relationship with matrix by means of SEM and TEM combined with EDS analysis, electron diffraction and central dark field imaging technique. The purpose is to clarify the controversies about coarse particles in Cu-Cr-Zr alloys and propose some suggestions for designing and processing of the system alloys.

## 2. Materials and Methods

Material with a composition of Cu-0.39Cr-0.24Zr-0.12Ni-0.027Si (wt.%) was melted using electrolytic copper, pure chromium, magnesium, silicon and copper-13 wt.% zirconium master alloy in a vacuum-induction melting furnace, and then cast in an iron mold with a size of  $35 \times 120 \times 180$  mm. The ingot was planed on both sides to remove surface defects and homogenized at 920 °C for 5 h and then hot rolled from 30 mm to 5 mm in thickness, followed by quickly quenching into cold water. Samples were cut and then solution-treated at 960 °C for 1 h in an air atmosphere muffle furnace.

Microstructure was characterized using an FEI Sirion 200 scanning electron microscope equipped with EDS. SEM image observations and EDS analyses of coarse particles were operated at a voltage of 15 kV. TEM specimens were mechanically thinned to 0.1 mm and punched into discs of 3 mm in diameter, and then thinned by jet polishing in a 30 vol.% nitric acid and 70 vol.% methanol solution at about  $-30$  °C. Microstructure observations, electron diffraction and energy dispersive analyses were carried out using a JEM 2100F transmission electron microscope with an accelerating voltage of 200 kV. Jade software was used to determine the crystal structure and lattice parameters, and CaRIne software was applied to construct the cells of the matrix and precipitated phases and simulate the crystal diffraction pattern under the specific zone axes.

## 3. Results

### 3.1. SEM Images and EDS Analysis Results of Coarse Particles in Cast Alloy

Figure 1 shows the SEM images and the results of the EDS analysis of coarse particles in cast Cu-Cr-Zr-Ni-Si alloy. It can be seen from the figure that there are a large number of dispersed micron particles both in the grain and at the grain boundary in the as-cast alloy. In the enlarged SEM image, near-spherical and short rod-like particles with a size of about 0.5–3  $\mu\text{m}$  can be observed, as indicated by the arrows in Figure 1b. The corresponding EDS analysis showed that these micron particles mainly contain Si, Cr, Ni and Cu elements.

### 3.2. SEM Images and EDS Analysis Results of Coarse Particles in Solution-Treated Alloy

Figure 2 shows the SEM images and EDS analysis results of Cu-Cr-Zr-Ni-Si alloy treated by solution. As can be seen from Figure 2a, after high-temperature solution treatment, the large number of micron particles which occurred in the as-cast alloy disappear, and only some coarse particles are distributed both in the grain and at the grain boundary, as shown in Figure 2a,b. This indicates that most of the as-cast micron particles were dissolved into the copper matrix during the high-temperature solution treatment. Two different characteristic particles can be observed in the backscattering electron image, as shown in Figure 2b. Bright white lath particle “A” with a length of about 3  $\mu\text{m}$  and a width of about 1.5  $\mu\text{m}$  was located inside the grains. The results of the EDS analysis showed that the particle is composed of elements of Si, Zr, Cr and Cu. The cross-sectional of dark black particle “B” exhibits a nearly circular shape, and mainly contains Cu, Cr and a small amount of Si (about 1.77 at. %). Since the contrast in a backscattering electron image relates to the atomic number (a conspicuous Z-contrast for  $\text{Fe}_x\text{Sn}_{1-x}/\text{MgO}$  can be seen due to the great difference in atomic numbers of Fe, Sn, Mg and O [30]), the contrast of particle A mainly contained Zr element (atomic number is 40) and is obviously brighter than particle B, which mainly contains Cr element (atomic number is 24).

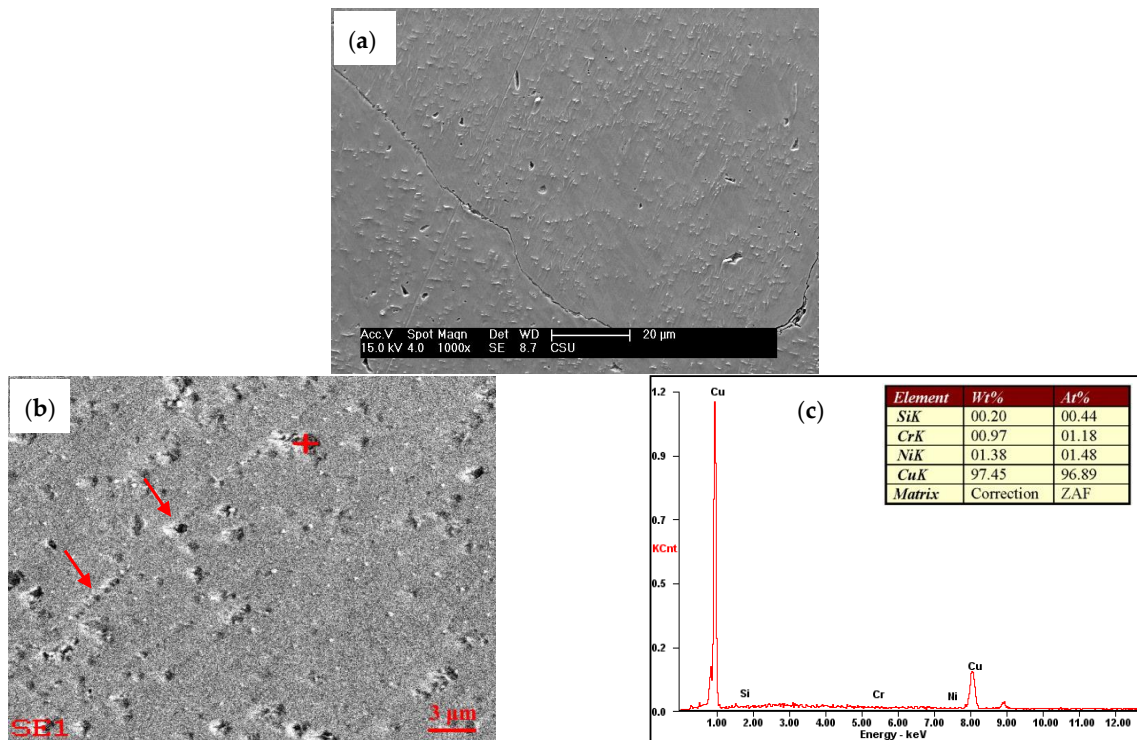


**Figure 1.** SEM images and EDS analysis results of coarse particles in cast Cu-Cr-Zr-Ni-Si alloy. (a) secondary electron image; (b) magnified secondary electron image; (c) EDS analysis results of selected particle in (b).

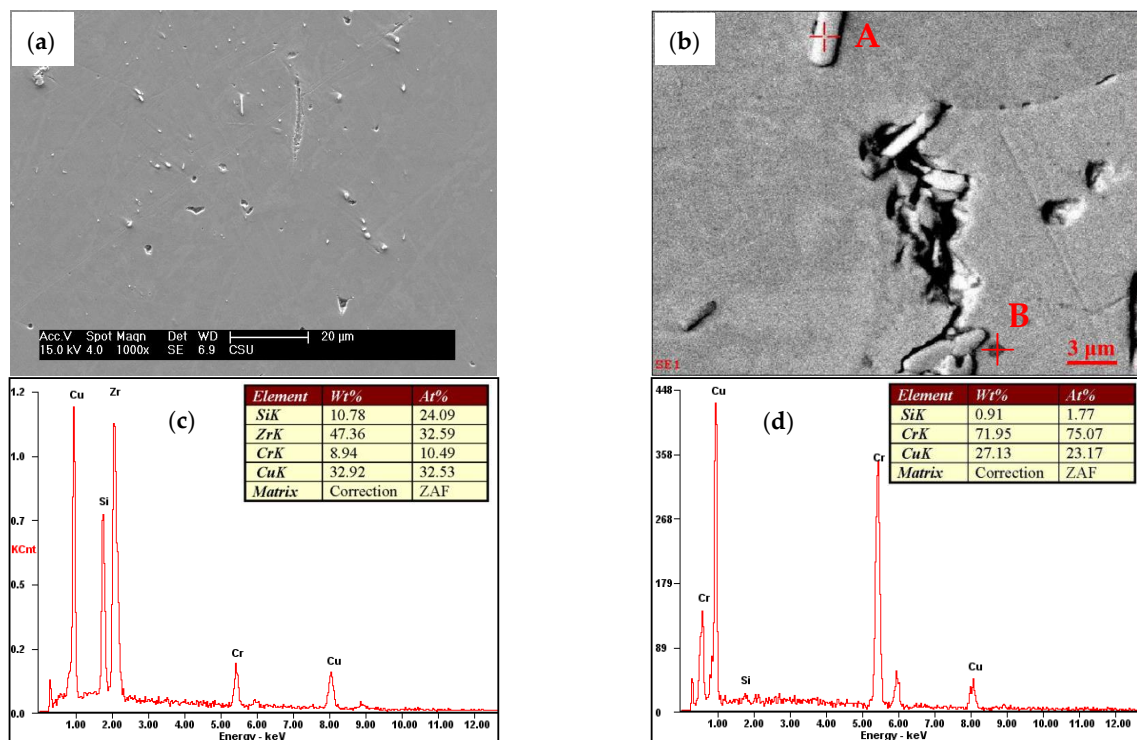


**Figure 2.** SEM image and EDS analysis results of coarse particles in solution-treated Cu-Cr-Zr-Ni-Si alloy. (a) secondary electron image in grain; (b) backscattering electron image at the grain boundary; (c) EDS analysis results of particle “A”; (d) EDS analysis results of particle “B”.

### 3.3. TEM Photographs and EDS Analysis Results of Coarse Particles in Solution-Treated Alloy

Figure 3 presents TEM photographs and EDS analysis results of coarse particles in the solution-treated Cu-Cr-Zr-Ni-Si alloy. It can be seen from Figure 3a that needle-like particles with a length of 100–200 nm (marked by red circle) grow from the grain boundary. The EDS analysis results indicate that the particles are a compound containing Cu and Zr elements. Figure 3c presents a nearly spherical phase with a size of about 200 nm in diameter, and it is proved to be a kind of (Si, Cr, Cu)-rich compound. In addition, a lath phase with a size of 300 nm × 100 nm, which mainly contains Si, Cr, Ni, Zr and Cu elements, can be observed inside the grains in Figure 3e. Similar results had been obtained from other samples which contain coarse particles with the same morphology. It can be inferred that the TEM and EDS analysis results on morphology and the contained elements of Figure 3 are consistent with those of the SEM and EDS analysis in Figure 2.

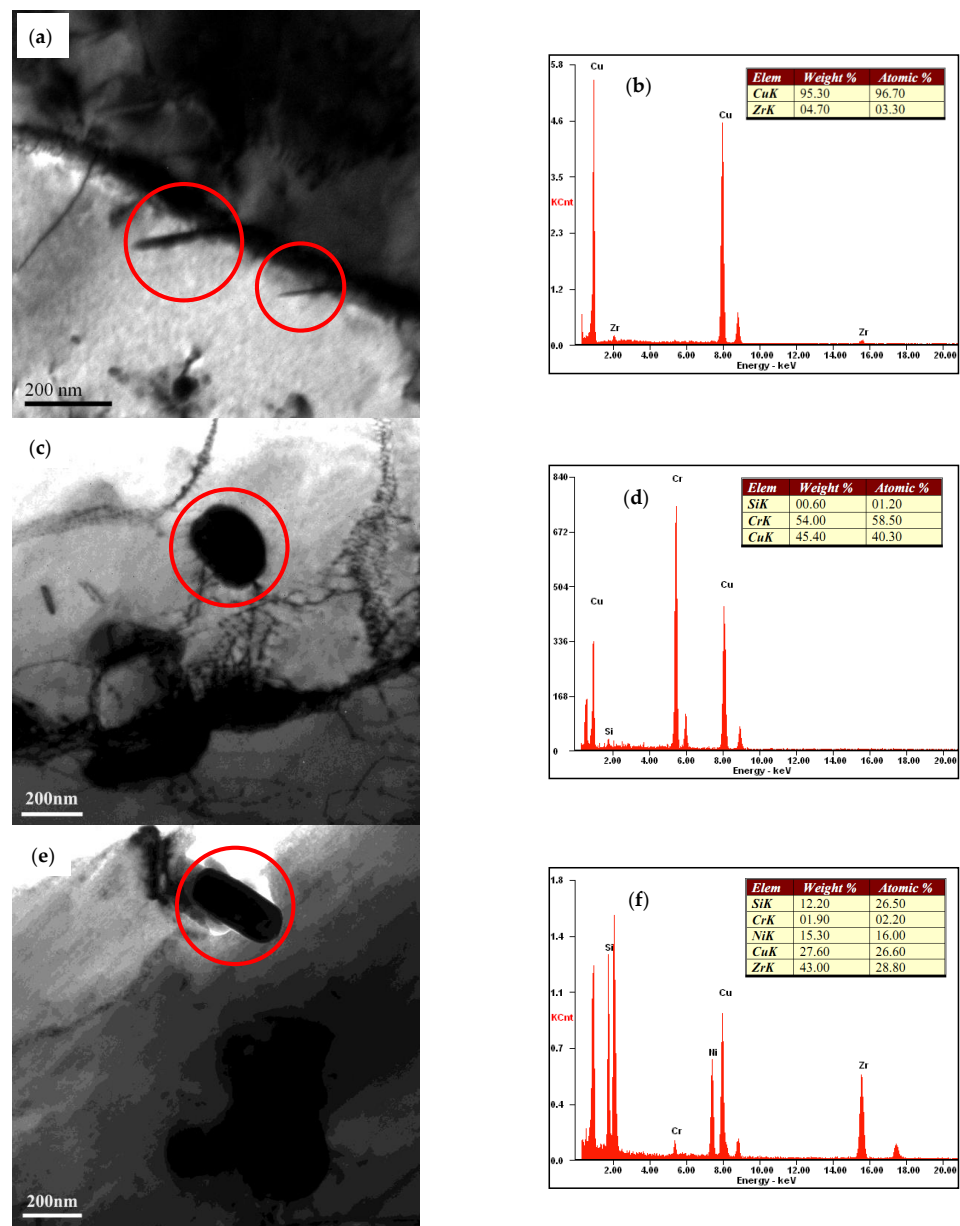


**Figure 3.** TEM images and EDS analysis results of coarse particles in solution-treated Cu-Cr-Zr-Ni-Si alloy. (a,b) needle-like particle and EDS analysis results; (c,d) nearly spherical particle and EDS analysis results; (e,f) lath-like particle and EDS analysis results.

### 3.4. TEM Images and Electron Diffraction Results of Coarse Particles in Solution-Treated Alloy

Figure 4 displays TEM images and the electron diffraction pattern of a coarse particle in the Cu-Cr-Zr-Ni-Si alloy. The bright field image and dark field image clearly show a needle-like particle that has a length of 820 nm and width of about 100 nm in Figure 4a, with the corresponding electron diffraction pattern shown in Figure 4c. Two sets of patterns can be distinguished from the electron diffraction pattern: one set of diffraction spots has higher intensity and smaller spacing between crystal planes, while the other set of diffraction spots shows slightly lower intensity and larger crystal face spacing. Angles between the adjacent diffracted spots and the transmitted spot of the two patterns were both measured to be about  $54^\circ$  and  $36^\circ$ , and the distance ratios were both determined to be about 1.1. The results fully comply with the diffraction pattern characteristic of f.c.c crystals under the  $\langle 011 \rangle$  zone axis. Therefore, it can be inferred that the two sets of diffraction patterns are both induced by f.c.c crystals under  $\langle 011 \rangle$  zone axes diffraction. The patterns were indexed as shown in Figure 4d. According to the spots distance, the lattice parameters of the two crystals were calculated as 0.3612 nm and 0.687 nm, respectively, and the two phases were identified with reference to the PDF card as follows: one is the Cu matrix and the other is the  $\text{Cu}_5\text{Zr}$  intermetallic phase, which belongs to  $\bar{F}43m$  (216) space group and has an f.c.c structure with a lattice parameter of 0.687 nm. The red-circled spot shown in Figure 4c was selected for an operation of central dark field, and the central dark field image is presented in Figure 4b. It can be further confirmed that the set of patterns is induced by the f.c.c structure  $\text{Cu}_5\text{Zr}$  intermetallic phase.

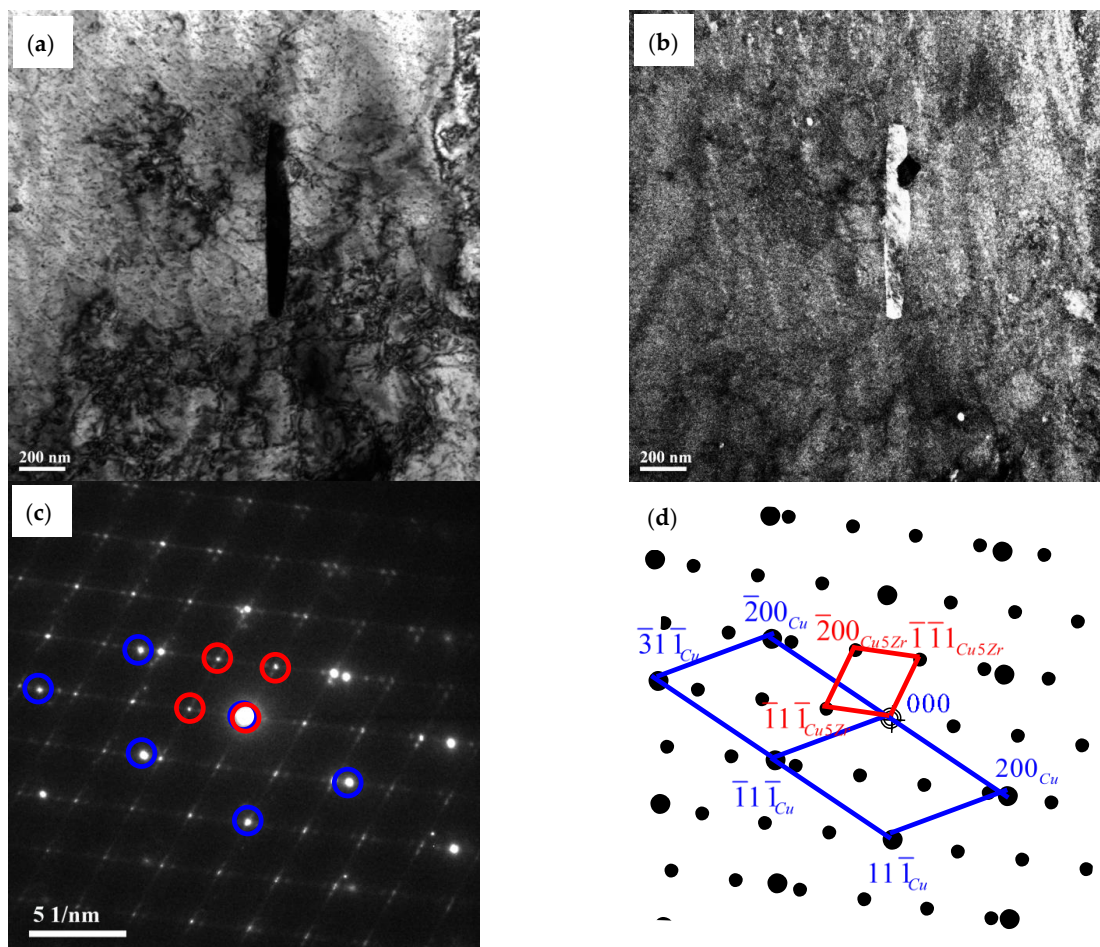


**Figure 4.** TEM images and electron diffraction pattern of needle-like particle in the Cu-Cr-Zr-Ni-Si alloy (● Cu; ○  $\text{Cu}_5\text{Zr}$ ). (a) bright filed image; (b) dark filed image; (c) electron diffraction pattern; (d) indexing result of (c).

According to the electron diffraction pattern and TEM bright field image, it can be ascertained that the  $\text{Cu}_5\text{Zr}$  phase grows along the  $\langle 111 \rangle$  direction of the Cu matrix. The orientation relationship between the  $\text{Cu}_5\text{Zr}$  phase and the matrix can also be determined as follows:  $[011]_{\text{Cu}} // [011]_{\text{Cu}_5\text{Zr}}$ ,  $(\bar{3}11)_{\text{Cu}} // (\bar{1}11)_{\text{Cu}_5\text{Zr}}$ .

Another nearly spherical particle with a size of approximately 40~120 nm in diameter can be observed in Figure 4. A bright field image and a dark field image of the particle are shown in Figure 5a,b, and the corresponding electron diffraction pattern is presented in Figure 5c. It can be inferred that the extra diffraction is caused by the  $\langle 001 \rangle$  zone axis of a b.c.c structure phase, and the lattice constant of the phase is 0.288 nm, calculated by the diffraction pattern. Based on the energy spectrum analysis results, which indicate a nearly spherical phase containing Cr and Si elements, it can be concluded that the extra diffraction is induced by a  $\text{Cr}_{9.1}\text{Si}_{0.9}$  intermetallic phase. The indexing result is shown in Figure 5d. According to the indexing result, a Nishiyama–Wassermann (N–W) orientation relationship can be found between the  $\text{Cr}_{9.1}\text{Si}_{0.9}$  phase and Cu matrix, which is that:  $[011]_{\text{Cu}} // [001]_{\text{Cr}_{9.1}\text{Si}_{0.9}}$ ,  $(\bar{1}11)_{\text{Cu}} // (\bar{1}10)_{\text{Cr}_{9.1}\text{Si}_{0.9}}$ ,  $(422)_{\text{Cu}} // (\bar{1}10)_{\text{Cr}_{9.1}\text{Si}_{0.9}} // (\bar{2}20)_{\text{Cr}_{9.1}\text{Si}_{0.9}}$ .

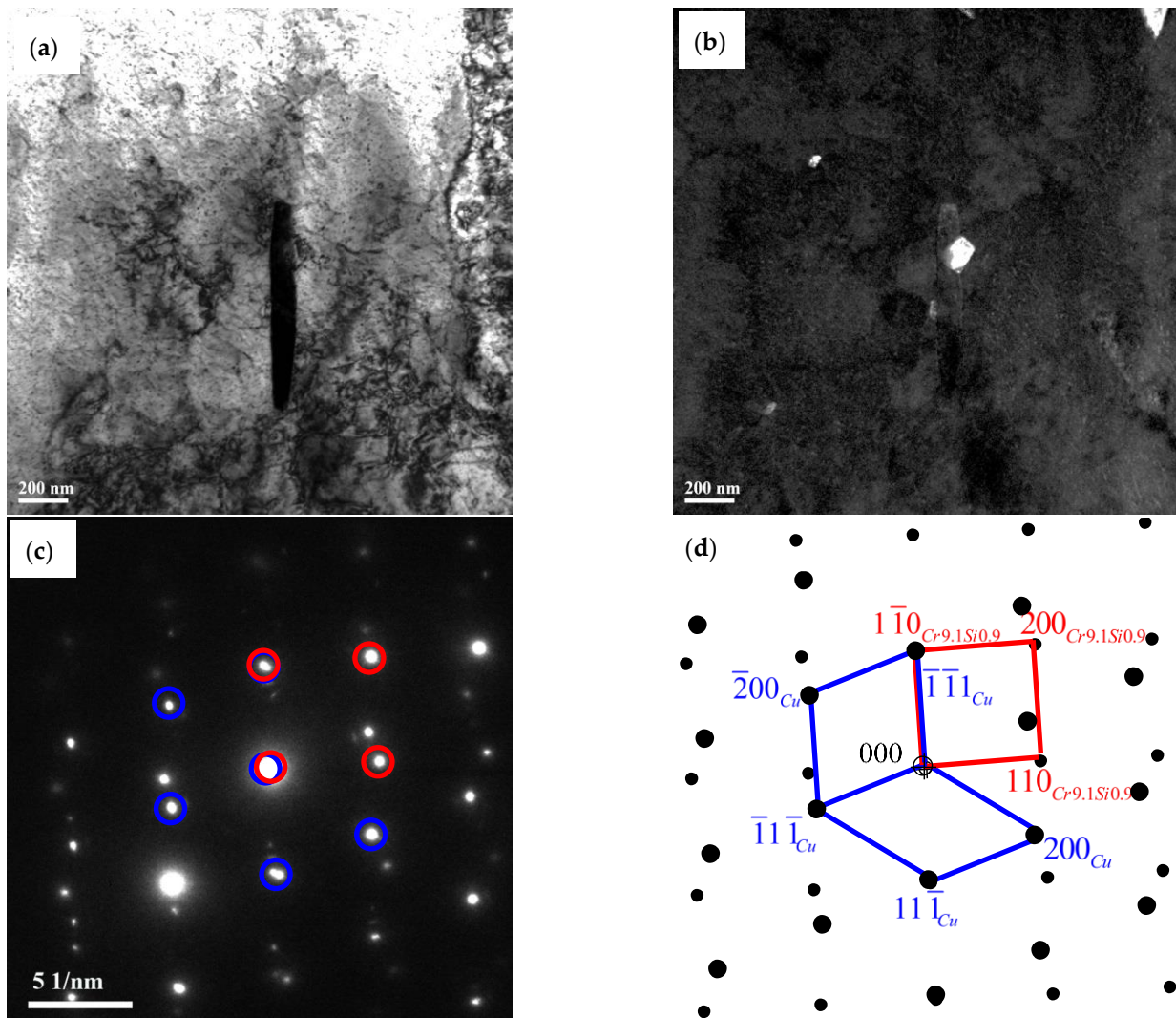


**Figure 5.** TEM images and electron diffraction pattern of nearly spherical phase in the Cu–Cr–Zr–Ni–Si alloy (○● Cu; ○●  $\text{Cr}_{9.1}\text{Si}_{0.9}$ ). (a) bright field image; (b) dark field image; (c) electron diffraction pattern; (d) indexing result of (c).

## 4. Discussion

### 4.1. The Determination of Coarse Particles in Cu-Cr-Zr System Alloys

Many investigations on the coarse particle types and their roles in Cu-Cr-Zr system alloys have been carried out by means of phase diagram theory, SEM, TEM and EDS, and great progress has been made. Batra et al. [19] investigated coarse particles with a size of about  $0.2 \mu\text{m} \times 0.4 \mu\text{m}$  in the Cu-Cr-Zr alloy by electron diffraction and concluded that the particles were b.c.c structure Cr particles. Club-shaped, hexagonal-shaped and spherical-shaped coarse particles were observed in Cu-0.43Cr-0.17Zr-0.05Mg-0.05RE alloy by Mu et al. [31], and EDS analysis showed that the coarse particles were Cr phase and (Cu, Zr) compound. Though the coarse Cr phase has been confirmed by most researchers, the type and structure of the (Cu, Zr) compounds is still uncertain. Kawakatsu et al. [32] studied the phase equilibrium at the copper corner of the isothermal diagram in Cu-Cr-Zr alloy and suggested that Zr existed in the form of  $\text{Cu}_3\text{Zr}$  in the alloy. Tang et al. [26] considered the coarse particles as a  $\text{Cu}_4\text{Zr}$  intermetallic phase in Cu-Cr-Zr-Mg alloy, but other's work on Cu-Cr-Zr alloy implied that  $\text{Cu}_{51}\text{Zr}_{14}$  should exist [27]. Theoretical studies [33] and SEM experimental studies [34] of Cu-Cr-Zr alloys showed that Cr phase and  $\text{Cu}_5\text{Zr}$  intermetallic phase should be present. These results accord well with those of Holzwarth [23], Correia [35] and Sun [36], who investigated the coarse particles in Cu-Cr-Zr alloy with SEM and EDS analysis.

Due to the spatial resolution limitation of electron microscopes in the mode of EDS (e.g., X-ray beam effectively analyzed by SEM-EDS can only be focused to a few hundred nanometers), the previous EDS studies on the coarse phase with a size of a few microns or a few hundred nanometers in Cu-Cr-Zr alloys could only show a qualitative result, and these failed to precisely determine the coarse particle types, structure and orientation relationship with the matrix. However, electron beams can be focused to a few nanometers in TEM electron diffraction mode, which greatly improves the accuracy and resolution of phase analysis.

The present work studied the presence of coarse particles in Cu-Cr-Zr-Ni-Si alloy as well as its chemical composition using SEM, TEM and corresponding EDS analysis, and established relations between the types and morphology of coarse particles. Three types of coarse particles were found in the Cu-Cr-Zr-Ni-Si alloy: needle-like (Cu, Zr) particles with a large aspect ratio, nearly spherical (Cu, Cr, Si) particles and lath (Cu, Cr, Zr, Ni, Si)-rich complex particles with a small aspect ratio. It can be inferred that the morphology of coarse particles varies with the composition.

Furthermore, the types, structure and crystallographic orientation relationships of the coarse particles were precisely examined using TEM electron diffraction and central dark field imaging techniques. Needle-like (Cu, Zr) particles were identified to be an f.c.c structure  $\text{Cu}_5\text{Zr}$  intermetallic phase, which belongs to space group  $\bar{F}43m$  (216) with a lattice parameter of 0.687 nm, having  $[011]_{\text{Cu}} // [011]_{\text{Cu}_5\text{Zr}}$ ,  $(\bar{3}11)_{\text{Cu}} // (111)_{\text{Cu}_5\text{Zr}}$  orientation relationship with matrix. The  $\text{Cu}_5\text{Zr}$  phase grows approximately along the  $\langle 111 \rangle$  direction of the copper matrix. As far as the authors know, this is the first time to show the selected area electron diffraction of  $\text{Cu}_5\text{Zr}$  intermetallic phase with a zone axis of [011] and determine the orientation relationship with the matrix. The nearly spherical (Cu, Cr, Si) particles were identified as  $\text{Cr}_{9.1}\text{Si}_{0.9}$  intermetallic phases with a b.c.c structure, which had a typical N-W orientation relationship with the matrix. The relationship is the same as the results reported by Luo [37], Dahmen [38] and Hall [39] in Cu-Cr alloys. From the bright field images and dark field images in Figures 4 and 5, it can also be found that a distinct interface exists between the  $\text{Cu}_5\text{Zr}$  phase and  $\text{Cr}_{9.1}\text{Si}_{0.9}$  phase. In addition, SEM and TEM results showed that the lath-like complex particles were composed of Si, Cr, Ni, Zr and Cu elements; however, these structure types and the orientation relationship need to be further studied.

#### 4.2. The Formation and Control of Coarse Particles in Cu-Cr-Zr System Alloys

The maximum solubility of the chromium and zirconium in equilibrium is 0.7 wt.% and 0.15 wt.% [40], respectively, and the solubility of chromium and zirconium in copper is less than 0.4 wt.% Cr and 0.15 wt.% Zr at 960 °C [41]. Since the composition of Cu-Cr-Zr-Ni-Si alloy is close to or above the solubility limit at the solution temperature, the coarse particles are almost formed during the solidification process. As can be seen from the results of this work, high-temperature solution treatment (960 °C for 1 h) failed to eliminate these coarse particles. The result that the dissolution of second particles was very limited by prolonging the high-temperature solution treatment can be confirmed by Appello [41]. Huang [27] suggested that the Cr-rich phase first solidified molten melt, and Zr-rich phase solidified at the interface of the Cr-rich phase and melt. In other words, the Cr-rich phase became as the solidified core of the Zr-rich phase. Spaic et al. [42] revealed that the Cr-rich phase was the eutectic reaction product formed in the solidification process, which explained the resistance against solution treatment.

It has been reported [43,44] that the second phase particles ranging from 1 nm to 100 nm have a significant strengthening effect on the mechanical properties of the material, so the coarse particles do not contribute to the mechanical strength of the Cu-Cr-Zr-Ni-Si alloy. Holzwarth [45] studied the mechanical properties of the Cu-Cr-Zr alloy under different heat treatment conditions and revealed that the differences in the density and spacing of the coarse particles had little effect on the mechanical properties. Furthermore, due to the difference in the deformation ability of coarse particles and the matrix, it is easy to generate stress concentration at the interface of coarse particles and matrix leading to the occurrence of fatigue and fractures in the hot-working or cold-working process. In addition, the formed coarse particles deplete the amount of solute elements dissolved in the matrix, resulting in the reduction in the precipitation strengthening effect. Therefore, controlling the amount and size of the coarse particles is essential for the precipitation-strengthened Cu-Cr-Zr system alloys. Effective measures can be taken as follows:

- (1) Reducing the content of alloying elements to ensure complete dissolution at the corresponding solution temperature according to the phase diagrams, e.g., the content of chromium element in the Cu-Cr-Zr alloys should be less than 0.3 wt.%, and zirconium should be less than 0.12 wt.% when the alloys are solution-treated at 920 °C.
- (2) Using master alloys instead of pure metals alloying elements for melting, which could accelerate alloying elements with high melting-point to melt and dissolve into the matrix.
- (3) Using modified treatment technology to refine precipitate particles formed in the solidification process.
- (4) Using severe plastic deformation in the hot-working or cold-working process, which could partly fragment the coarse particles and redistribute the alloying elements, ultimately relieving the negative effects of coarse particles on the performance of Cu-Cr-Zr alloys.

#### 5. Conclusions

- (1) Three types of coarse particles were detected in the Cu-Cr-Zr-Ni-Si alloy and the relations between types, composition and morphology of coarse particles were also established.
- (2) Needle-like (Cu, Zr) particles were accurately determined to be an f.c.c structure  $\text{Cu}_5\text{Zr}$  intermetallic phase, and the orientation relationship between the  $\text{Cu}_5\text{Zr}$  phase and Cu matrix was determined as  $[011]_{\text{Cu}} // [011]_{\text{Cu}_5\text{Zr}}, (\bar{3}11)_{\text{Cu}} // (\bar{1}11)_{\text{Cu}_5\text{Zr}}$ .
- (3) Nearly spherical particles were identified as a  $\text{Cr}_{9.1}\text{Si}_{0.9}$  intermetallic phase with a b.c.c structure, having a typical N–W orientation relationship with the Cu matrix. Another coarse particle with a lath shape was confirmed as a kind of (Cu, Cr, Zr, Ni, Si)-rich complex compound.

**Author Contributions:** Conceptualization, C.X. and Y.P.; methodology, Y.P. and Y.J.; validation, S.D. and W.Z.; formal analysis, C.X., C.N. and Y.P.; investigation, S.D. and W.Z.; resources, Y.J.; data curation, S.D. and W.Z.; writing—original draft preparation, C.X.; writing—review and editing, C.N., Y.P. and Y.J.; visualization, S.D. and W.Z.; supervision, Y.J.; project administration, C.X. and C.N.; funding acquisition, C.X. and C.N. All authors have read and agreed to the published version of the manuscript.

**Funding:** This research was funded by the Joint Funds of the Zhejiang Provincial Natural Science Foundation of China (Grant No. LZY23E010001 and LZY22E010002), Zhejiang College Students Innovation and Entrepreneurship Training Program (2022R435A004).

**Institutional Review Board Statement:** Not applicable.

**Informed Consent Statement:** Not applicable.

**Data Availability Statement:** The data used to support the findings of this study are available from the corresponding author upon request.

**Conflicts of Interest:** The authors declare no conflict of interest.

## References

1. Chen, J.; Xiao, X.; Yuan, D.; Guo, C.; Huang, H.; Yang, B. Microstructure and properties of Cu-Cr-Zr alloy with columnar crystal structure processed by upward continuous casting. *J. Alloys Compd.* **2021**, *889*, 161700. [[CrossRef](#)]
2. Mao, Q.; Zhang, Y.; Guo, Y.; Zhao, Y. Enhanced electrical conductivity and mechanical properties in thermally stable fine-grained copper wire. *Commun. Mater.* **2021**, *2*, 46. [[CrossRef](#)]
3. Zhou, Y.; Zheng, C.; Chen, J.; Chen, A.; Jia, L.; Xie, H.; Lu, Z. Characterizations on Precipitations in the Cu-Rich Corner of Cu-Ni-Al Ternary Phase Diagram. *Crystals* **2023**, *13*, 274. [[CrossRef](#)]
4. Li, S.; Fang, M.; Xiao, Z.; Meng, X.; Lei, Q.; Jia, Y. Effect of Cr addition on corrosion behavior of cupronickel alloy in 3.5 wt% NaCl solution. *J. Mater. Res. Technol.* **2023**, *22*, 2222–2238. [[CrossRef](#)]
5. Ding, Y.; Xiao, Z.; Fang, M.; Gong, S.; Dai, J. Microstructure and mechanical properties of multi-scale  $\alpha$ -Fe reinforced Cu-Fe composite produced by vacuum suction casting. *Mater. Sci. Eng. A* **2023**, *864*, 144603. [[CrossRef](#)]
6. Ma, M.; Zhang, X.; Li, Z.; Xiao, Z.; Jiang, H.; Xia, Z.; Huang, H. Effect of Equal Channel Angular Pressing on Microstructure and Mechanical Properties of a Cu-Mg Alloy. *Crystals* **2020**, *10*, 426. [[CrossRef](#)]
7. Guo, T.; Tai, X.; Wei, S.; Wang, J.; Jia, Z.; Ding, Y. Microstructure and Properties of Bulk Ultrafine-Grained Cu<sub>1.5</sub>Cr<sub>0.1</sub>Si Alloy through ECAP by Route C and Aging Treatment. *Crystals* **2020**, *10*, 207. [[CrossRef](#)]
8. Zhang, Y.; Volinsky, A.A.; Hai, T.T.; Chai, Z.; Liu, P.; Tian, B.; Liu, Y. Aging behavior and precipitates analysis of the Cu-Cr-Zr-Ce alloy. *Mater. Sci. Eng. A* **2016**, *650*, 248–253. [[CrossRef](#)]
9. Li, J.; Ding, H.; Li, B.; Wang, L. Microstructure evolution and properties of a Cu-Cr-Zr alloy with high strength and high conductivity. *Mater. Sci. Eng. A* **2021**, *819*, 141464. [[CrossRef](#)]
10. Huang, A.H.; Wang, Y.F.; Wang, M.S.; Song, L.Y.; Zhu, Y.T. Optimizing the strength, ductility and electrical conductivity of a Cu-Cr-Zr alloy by rotary swaging and aging treatment. *Mater. Sci. Eng. A* **2019**, *746*, 211–216. [[CrossRef](#)]
11. Wang, Y.D.; Liu, M.; Yu, B.H.; Wu, L.H.; Xue, P.; Ni, D.R.; Ma, Z.Y. Enhanced combination of mechanical properties and electrical conductivity of a hard state Cu-Cr-Zr alloy via one-step friction stir processing. *J. Mater. Process. Technol.* **2021**, *288*, 116880. [[CrossRef](#)]
12. Sousa, T.G.; Moura, I.A.D.B.; Filho, F.D.C.G.; Monteiro, S.N.; Brandão, L.P. Combining severe plastic deformation and precipitation to enhance mechanical strength and electrical conductivity of Cu-0.65Cr-0.08Zr alloy. *J. Mater. Res. Technol.* **2020**, *9*, 5953–5961. [[CrossRef](#)]
13. Xia, C.; Zhang, W.; Kang, Z.; Jia, Y.; Wu, Y.; Zhang, R.; Xu, G.; Wang, M. High strength and high electrical conductivity Cu-Cr system alloys manufactured by hot rolling-quenching process and thermomechanical treatments. *Mater. Sci. Eng. A* **2012**, *538*, 295–301. [[CrossRef](#)]
14. Xia, C.; Wang, M.; Zhang, W.; Kang, Z.; Jia, Y.; Zhang, R.; Yu, H. Microstructure and properties of a hot rolled-quenched Cu-Cr-Zr-Mg-Si alloy. *J. Mater. Eng. Perform.* **2012**, *21*, 1800–1805. [[CrossRef](#)]
15. Xia, C.; Jia, Y.; Zhang, W.; Zhang, K.; Dong, Q.Y.; Xu, G.; Wang, M. Study of deformation and aging behaviors of a hot rolled-quenched Cu-Cr-Zr-Mg-Si alloy during thermomechanical treatments. *Mater. Des.* **2012**, *39*, 404–409. [[CrossRef](#)]
16. Pang, Y.; Xia, C.; Wang, M.; Li, Z.; Xiao, Z.; Wei, H.; Chen, C. Effects of Zr and (Ni, Si) additions on properties and microstructure of Cu-Cr alloy. *J. Alloys Compd.* **2014**, *582*, 786–792. [[CrossRef](#)]
17. Cheng, J.Y.; Shen, B.; Yu, F.X. Precipitation in a Cu-Cr-Zr-Mg alloy during aging. *Mater. Charact.* **2013**, *81*, 68–75. [[CrossRef](#)]
18. Peng, L.; Xie, H.; Huang, G.; Xu, G.; Yin, X.; Feng, X.; Mi, X.; Yang, Z. The phase transformation and strengthening of a Cu-0.71wt% Cr alloy. *J. Alloys Compd.* **2017**, *708*, 1096–1102. [[CrossRef](#)]
19. Batra, I.S.; Dey, G.K.; Kulkarni, U.D.; Banerjee, S. Precipitation in a Cu-Cr-Zr alloy. *Mater. Sci. Eng. A* **2002**, *356*, 32–36. [[CrossRef](#)]

20. Fujii, T.; Nakazawa, H.; Kato, M.; Dahmen, U. Crystallography and morphology of nanosized Cr particles in Cu-0.2%Cr alloy. *Acta Mater.* **2000**, *48*, 1033–1045.
21. Chbihi, A.; Sauvage, X.; Blavette, D. Atomic scale investigation of Cr precipitation in copper. *Acta Mater.* **2012**, *60*, 4575–4585. [[CrossRef](#)]
22. Xia, C.; Pang, Y.; Jia, Y.; Ni, C.; Sheng, X.; Wang, S.; Jiang, X.; Zhou, Z. Orientation relationships between precipitates and matrix and their crystallographic transformation in a Cu–Cr–Zr alloy. *Mater. Sci. Eng. A* **2022**, *850*, 143576. [[CrossRef](#)]
23. Holzwarth, U.; Stamm, H. The precipitation behaviour of ITER-grade Cu–Cr–Zr alloy after simulating the thermal cycle of hot isostatic pressing. *J. Nucl. Mater.* **2000**, *279*, 31–45. [[CrossRef](#)]
24. Morris, M.A.; Leboeuf, M.; Morris, D.G. Recrystallization mechanisms in a Cu–Cr–Zr alloy with a bimodal distribution of particles. *Mater. Sci. Eng. A* **1994**, *188*, 255–265. [[CrossRef](#)]
25. Suzuki, H.; Kanno, M.; Kawakatsu, I. Strength of Cu–Cr–Zr alloy relating to the aged structures. *J. Jpn. Inst. Met.* **1969**, *33*, 628–633. [[CrossRef](#)]
26. Tang, N.Y.; Taplin, D.M.R.; Dunlop, G.L. Precipitation and aging in high-conductivity Cu–Cr alloys with additions of zirconium and magnesium. *Mater. Sci. Technol.* **1985**, *1*, 270–275. [[CrossRef](#)]
27. Huang, F.; Ma, J.; Ning, H.; Geng, Z. Analysis of phases in a Cu–Cr–Zr alloy. *Scr. Mater.* **2003**, *48*, 97–102.
28. Ge, L.; Hui, X.; Wang, E.R.; Chen, G.L.; Arroyave, R.; Liu, Z.K. Prediction of the glass forming ability in Cu–Zr binary and Cu–Zr–Ti ternary alloys. *Intermetallics* **2008**, *16*, 27–33. [[CrossRef](#)]
29. Cui, X.; Zu, F.Q.; Wang, Z.Z.; Huang, Z.Y.; Li, X.Y.; Wang, L.F. Study of the reversible intermetallic phase: B2-type CuZr. *Intermetallics* **2013**, *36*, 21–24. [[CrossRef](#)]
30. Myagkov, V.G.; Zhigalov, V.S.; Bykova, L.E.; Solovyov, L.A.; Matsynin, A.A.; Balashov, Y.; Nemtsev, I.V.; Shabanov, A.V.; Bondarenko, G.N. Solid-state synthesis, dewetting, and magnetic and structural characterization of interfacial Fe<sub>x</sub>Sn<sub>1-x</sub> layers in Sn/Fe(001) thin films. *J. Mater. Res.* **2021**, *36*, 3121–3133. [[CrossRef](#)]
31. Mu, S.G.; Guo, F.A.; Tang, Y.Q.; Cao, X.M.; Tang, M.T. Study on microstructure and properties of aged Cu–Cr–Zr–Mg–RE alloy. *Mater Sci Eng A* **2008**, *475*, 235–240. [[CrossRef](#)]
32. Kawakatsu, I.; Suzuki, H.; Kitano, H. Properties of high zirconium Cu–Zr–Cr alloys and their isothermal diagram of the copper corner. *J. Jpn. Inst. Met.* **1967**, *31*, 1253–1257. [[CrossRef](#)]
33. Zeng, K.J.; Hamalainen, M. A theoretical study of the phase equilibria in the Cu–Cr–Zr system. *J. Alloys Compd.* **1995**, *220*, 53–61. [[CrossRef](#)]
34. Zeng, K.J.; Hamalainen, M.; Lilius, K. Phase relationships in Cu-rich corner of the Cu–Cr–Zr phase diagram. *Scr. Metall. Mater.* **1995**, *32*, 2009–2014. [[CrossRef](#)]
35. Correia, J.B.; Davies, H.A.; Sellars, C.M. Strengthening in rapidly solidified age hardened Cu–Cr and Cu–Cr–Zr alloys. *Acta Mater.* **1997**, *45*, 177–190. [[CrossRef](#)]
36. Sun, Z.; Guo, J.; Song, X.; Zhu, Y.; Li, Y. Effects of Zr addition on the liquid phase separation and the microstructures of Cu–Cr ribbons with 18–22at.% Cr. *J. Alloys Compd.* **2008**, *455*, 243–248. [[CrossRef](#)]
37. Luo, C.P.; Dahmen, U.; Westmacott, K.H. Morphology and crystallography of Cr precipitates in a Cu-0.33 wt% Cr alloy. *Acta Metall. Mater.* **1994**, *42*, 1923–1932. [[CrossRef](#)]
38. Dahmen, U. Orientation relationships in precipitation systems. *Acta Metall.* **1982**, *30*, 63–73. [[CrossRef](#)]
39. Hall, M.G.; Aaronson, H.I.; Kinsma, K.R. The structure of nearly coherent fcc: Bcc boundaries in a Cu–Cr alloy. *Surf. Sci.* **1972**, *31*, 257–274. [[CrossRef](#)]
40. Chakrabarti, D.J.; Laughlin, D.E. The Cr–Cu (chromium–copper) system. *Bull. Alloy Phase Diagr.* **1984**, *5*, 59–68. [[CrossRef](#)]
41. Appello, M.; Fenici, P. Solution hot treatment of a CuCrZr alloys. *Mater. Sci. Eng. A* **1988**, *102*, 69–75. [[CrossRef](#)]
42. Spaic, S.; Krizman, A.; Marinkovic, V. Structure and properties of low-alloy, hardenable copper alloys. *Metall* **1985**, *39*, 43–48.
43. Martin, J.W. *Micromechanisms in Particle-Hardened Alloys*, 1st ed.; Cambridge University Press: Cambridge, UK, 1980.
44. Lee, S.; Matsunaga, H.; Sauvage, X.; Horita, Z. Strengthening of Cu–Ni–Si alloy using high-pressure torsion and aging. *Mater. Charact.* **2014**, *90*, 62–70. [[CrossRef](#)]
45. Holzwarth, U.; Pisoni, M.; Scholz, R.; Stamm, H.; Volcan, A. On the recovery of the physical and mechanical properties of a CuCrZr alloy subjected to heat treatments simulating the thermal cycle of hot isostatic pressing. *J. Nucl. Mater.* **2000**, *279*, 19–30. [[CrossRef](#)]

**Disclaimer/Publisher’s Note:** The statements, opinions and data contained in all publications are solely those of the individual author(s) and contributor(s) and not of MDPI and/or the editor(s). MDPI and/or the editor(s) disclaim responsibility for any injury to people or property resulting from any ideas, methods, instructions or products referred to in the content.